

20 Optical Properties of Solids and Nanostructures from a Many-Body f_{xc} Kernel

A. Marini, R. Del Sole, and A. Rubio

20.1 Introduction

Until the late 1990's, the situation for the ab initio calculation of optical properties of real materials was not nearly as good as that for the quasiparticle properties. As already mentioned in Chap. 10, the description of the optical response of an interacting electron system asks for the inclusion of effects beyond single-particle excitations as electron-hole interactions (excitonic effects). The important consequence of such effects is illustrated below for many different semiconductors and insulators by comparing the computed absorption spectrum neglecting electron-hole interaction with the experimental spectrum. For wide band-gap insulators there is hardly any resemblance between the spectrum from the noninteracting theory to that of experiment.

In contrast to the many-body Bether-Salpeter scheme¹, TDDFT using the standard local and semilocal xc functionals has a number of commonly invoked failures. One example is the difficulty encountered when studying extended systems; another one is the severe underestimation of high-lying excitation energies in molecules. For example, the fact that the strong nonlocality of the exact functional is not captured by the usual approximations for xc leads to a very poor description of the polarisability per unit-length of long-conjugated molecular chains. As we will see below, the main reason of this deficiency is related to the long-range nature of the xc kernel [Onida 2002]. Indeed, the advances in the development of functionals during the last years based on many-body perturbation theory and other schemes (see contributions to Part I), have broadened the field of applicability of TDDFT, as demonstrated by the variety of examples presented in this chapter.

Before discussing the applications of the many-body f_{xc} kernel, it is important to highlight the intrinsic pathologies that should be present in DFT, and that are naturally incorporated into a many-body scheme. We know that the actual functional relation between $n(\mathbf{r})$ and $v_{xc}(\mathbf{r})$ is highly nonanalytical and highly nonlocal. Some specific problems related to this inherent nonlocalities of the xc functional relevant for the description of optical properties are:

¹ The Bethe-Salpeter scheme is based on approximating the electron self-energy by the GW approximation and solving the two-particle Bethe-Salpeter equation; see Chap. 10 for more details.

(i) The band-gap in the local density functional theory (Kohn-Sham gap E_g) is typically 30–50% less than the observed band-gap. This so-called band-gap problem is related to the discontinuity of the xc potential with respect to the number of particles [Perdew 1983, Sham 1983]. (ii) The macroscopic xc electric field [Gonze 1995b, Gonze 1997b, Gonze 1997a, Resta 1994, Ortiz 1998], which is related to the spatial nonlocality of the xc-potential. Similarly, the description of how excitonic effects modify the shape and pole-structure of the Kohn-Sham system needs nonlocal and, most likely, frequency dependent xc kernels. A many-body Bethe-Salpeter approach handles properly all those effects and, therefore, provides some guidelines about how to incorporate many-body effects into the xc kernel f_{xc} in order to properly describe the optical spectra of extended and low-dimensional systems (as illustrated, for example, in Chap. 10 of this book).

In this chapter we review the results recently obtained by different groups [Onida 2002, Reining 2002, Sottile 2003, Adragna 2003, Marini 2003b, Marini 2004, Botti 2004, Del Sole 2003, Bruneval 2005] using the many-body derived xc kernel presented in Chap. 10. In particular, we focus the discussion on results within linear response theory for the optical absorption and loss function of extended solids and low-dimensional structures. As a particular case, the new derived kernels reproduce the exact-exchange results of [Kim 2002a, Kim 2002b] obtained by turning-off the screening in the building-up process of the f_{xc} kernel. Following Chap. 10 we focus the discussion here on how can an f_{xc} mimic the electron-hole interaction contribution, absorbing the quasiparticle self-energy shifts in the eigenvalues of our starting independent Kohn-Sham response function χ_{KS} (see discussion in Chap. 10 for details).

We decided to present the results in terms of the dimensionality of the system under study. The idea behind is to show clearly that the many-body derived f_{xc} is able to reproduce the results obtained from the solution of the many-body Bethe-Salpeter equation, not only for solids but also for molecules, polymers and surfaces. In this way, we provide compelling evidence about the robustness and wide-range of applicability of the new xc kernel and lays down the basic ingredients to build a fully DFT-based approach. Work along those lines is in progress using a variational many-body total energy functionals [Almbladh 1999, Dahlen 2005] in either an optimised effective potential (OEP) or generalized Kohn-Sham scheme² [Gruning 2005].

20.2 Applications to Solids and Surfaces

In Chap. 10 a many-body xc kernel f_{xc} was derived by taking as reference the Bethe-Salpeter equation. The kernel is, in principle, nonlocal both in space

² The simplest case are functionals derived from the GW approximation to the electron self-energy and that correspond to the so-called random-phase approximation (RPA)-total energy functionals.

and time. However, by looking at the leading terms of this kernel a simple static long range correction (LRC) model was derived [Reining 2002]:

$$f_{xc}^{\text{LRC}}(\mathbf{q}, \mathbf{G}, \mathbf{G}') = -\delta_{\mathbf{G}, \mathbf{G}'} \frac{\alpha}{|\mathbf{q} + \mathbf{G}|^2}, \quad (20.1)$$

where α is a suitable constant. It is illustrative to see how this simple LRC model suffices to get a proper optical spectra for a wide range of solids. It has been shown [Onida 2002, Reining 2002, Sottile 2003, Botti 2004] that the optical absorption spectrum of solids exhibiting a strong continuum excitonic effect is considerably improved with respect to calculations where the adiabatic local-density approximation is used. However, there are limitations of this simple approach, and in particular the same improvement cannot be found for the whole spectral range including the valence plasmons and bound excitons. For this, a full solution of the many-body kernel including all coupling-terms is needed [Marini 2003b, Reining 2002, Sottile 2003, Olevano 2001]. The frequency dependence of f_{xc} has been clearly shown in [Adragna 2003]. Still, for semiconductors with no strong excitonic effect a simple dynamical extension of the LRC model has been put forward by [Botti 2005].³

The advantage of this dynamical model is that both absorption and loss-spectra are covered with the same set of parameters, however for insulators with strong electron-hole effects one has to resort to the solution of the full many-body f_{xc} .

Applications of the LRC model have been performed [Botti 2004] for the real and the imaginary part of the dielectric function of bulk silicon, gallium arsenide, aluminum arsenide, diamond, magnesium oxide and silicon carbide, and for the loss function of silicon. A summary of those results is presented in Figs. 20.1, 20.2, and 20.3. The dot-dashed curves stem from a standard TDLDA calculation. The TDLDA results are close to the RPA one, showing the well-known discrepancies with experiment: peak positions are wrong (the TDDFT spectrum is redshifted), and the intensity of the first main structure (the E_1 peak in Si, GaAs and AlAs) is strongly underestimated. The dashed curve (named GW-RPA) is the result obtained by replacing KS eigenvalues with GW quasiparticle energies in the RPA screening. The calculated spectrum is now blue shifted. Moreover, the lineshape has not been corrected. Finally, the continuous curve is the result of the TDDFT calculation using the LRC xc kernel. An excellent fit to experiment is obtained using $\alpha = 0.22$, 0.2, and 0.35 for Si, GaAs and AlAs, respectively. There is a clear dependence of the parameter α on the material. As one would expect, α is approximately inversely proportional to the screening in the material. This fact can give a hint of how to estimate the excitonic correction to an absorption spectrum for a material where one has not yet solved the Bethe-Salpeter equation

³ The form of the dynamical-model for the kernel is: $f_{xc} = -\frac{\alpha + \beta\omega^2}{q^2}$, with α and β related to the macroscopic dielectric constant and bulk plasma frequency.

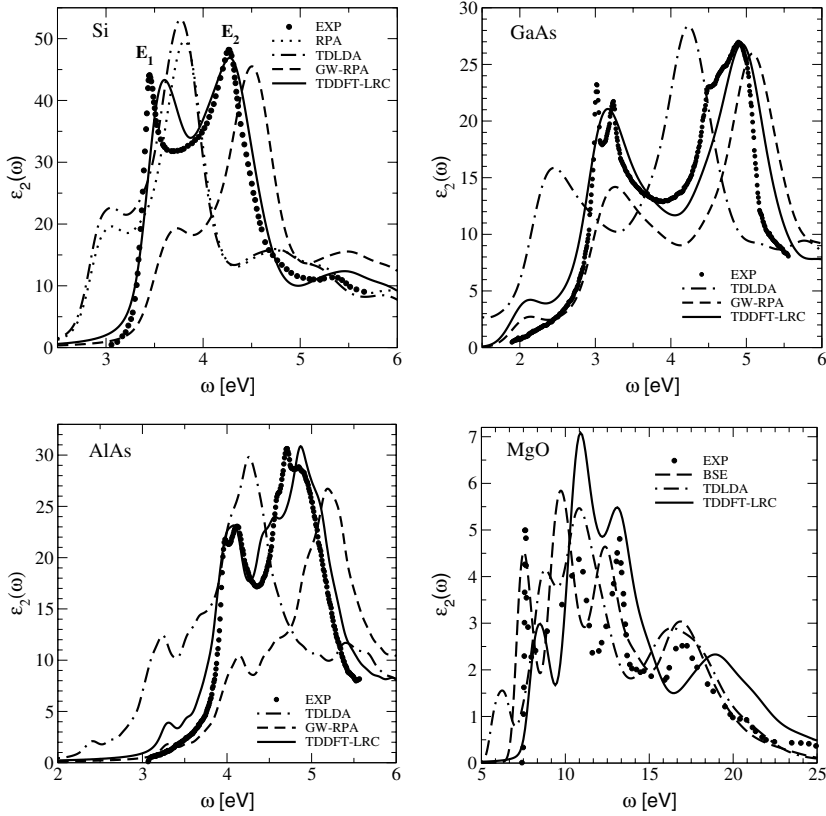


Fig. 20.1. Calculated absorption spectra of different semiconductors and insulators. Panel (a) is silicon, (b) GaAs, (c) AlAs, and (d) MgO. *Dots*: experimental data. *Dot-dashed curve*: TDLDA result. *Dashed curve*: GW-RPA (i.e., standard RPA calculation using the GW-quasiparticle energies instead of the Kohn-Sham ones). *Continuous curve*: TDDFT result using the LRC approximation to the kernel (Adapted from [Botti 2004])

(see [Botti 2004] for more details). In particular, we can estimate the spectra of new compounds as semiconducting alloys (“computational alchemy”).

Similar agreement is found for the real part of the dielectric function. This fact is illustrated considering the case of GaAs as example (see Figs. 20.1 and 20.2). We see that even for this simple and well-known semiconductor, only with the inclusion of electron-hole interaction we have good agreement between theory and experiment. The influence of the electron-hole interaction extends over an energy range far above the fundamental band gap. As seen from the figure, the optical strength of GaAs is enhanced by nearly a factor of two in the low frequency regime. Also, the electron-hole interaction enhances and shifts the second prominent peak (the so-called E_2 peak) structure at 5 eV

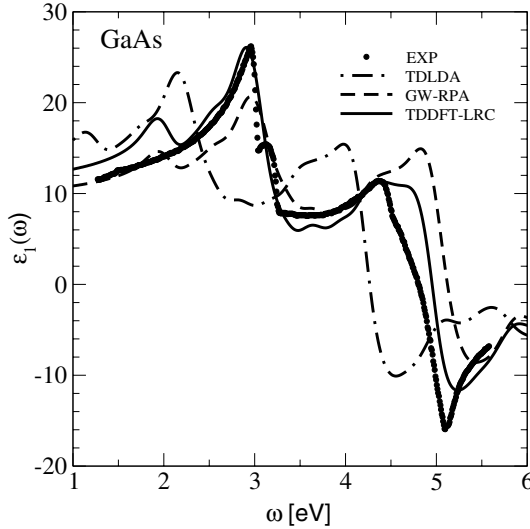


Fig. 20.2. Real part of the macroscopic dielectric response of GaAs computed within the different approximations discussed in the main text and compared to experiments. The labeling is the same as the one in Fig. 20.1

to a value much closer to experiment. This very large shift of about 0.5 eV is not due to a negative shift of the transition energies, as one might naïvely expect from an attractive electron-hole interaction. The changes in the optical spectrum originate mainly from the coupling of different electron-hole configurations in the excited states, which leads to a constructive coherent superposition of the interband transition oscillator strengths for transitions at lower energies and to a destructive superposition at energies above 5 eV [Rohlfing 1998a].

When going to large-gap materials, the screening is smaller and the electron-hole interaction becomes stronger. One can therefore expect that this drastic LRC approximation to the full kernel will break down (indeed this is the case for systems having bound excitons, see below and [Marini 2003b]). This can be clearly seen in Fig. 20.1 for MgO. In this case, the choice of $\alpha = 1.8$ is a compromise which allows to enhance the first excitonic peak to a good fraction of the experimental value, without overestimating too much the strength of the subsequent structures.

From the previous discussion we conclude that low energy part of the macroscopic dielectric function of many semiconductors is extremely well reproduced when just the long-range contribution for the xc kernel is taken into account, whereas the *same* long-range contribution cannot yield good results for the loss function (see Fig. 20.3). The role of long-range interactions

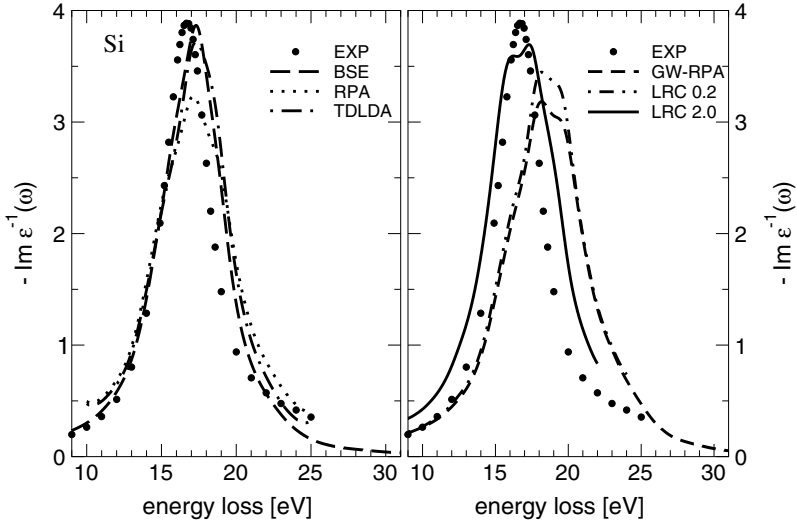


Fig. 20.3. Calculated energy-loss function of Si from different approximation to the xc kernel: RPA, TDLDA, Bethe-Salpeter (BSE) and LRC-model (adapted from [Olevano 2001, Botti 2004]). Two values of the LRC model are used, the one that describes the absorption spectra ($\alpha = 0.2$) does not reproduces the loss function that requires a larger value of the constant $\alpha = 2$. The experimental data is given by the *dots*

is fundamentally different in the loss spectra, and one can expect that a small long-range contribution to the kernel will have much less effect than in the case of absorption spectra. Figure 20.3 demonstrates the quite general finding that, in the case of loss spectra, both the RPA (dotted curve) and, even better, the TDLDA (dot-dashed curve), already manage to reproduce reasonably the experimental results (dots) [Olevano 2001] (the Bethe-Salpeter results are also given for completeness; dashed curve). As expected the one-parameter LRC approach breaks down for this application. The dot-dashed curve of the bottom panel of Fig. 20.3 shows the LRC result using the same $\alpha = 0.22$ as for the absorption spectrum. Almost no effect is seen on the loss spectrum, and one is thus left essentially with the rather unsatisfying GW-RPA result. Instead, using the much larger value $\alpha = 2$ (continuous curve), the result is again satisfactory⁴. Therefore, this implies that if one is interested in a large frequency range, the full many-body kernel derived in Chap. 10 should be used. In that case we will recover the same level of accuracy as the Bethe-Salpeter calculations (see below for some results obtained for LiF [Marini 2003b]).

⁴ This is the result that one would obtain by using the dynamical extension of the LRC model as done in [Botti 2005] for Si using the same set of parameters for both absorption and electron energy loss spectra.

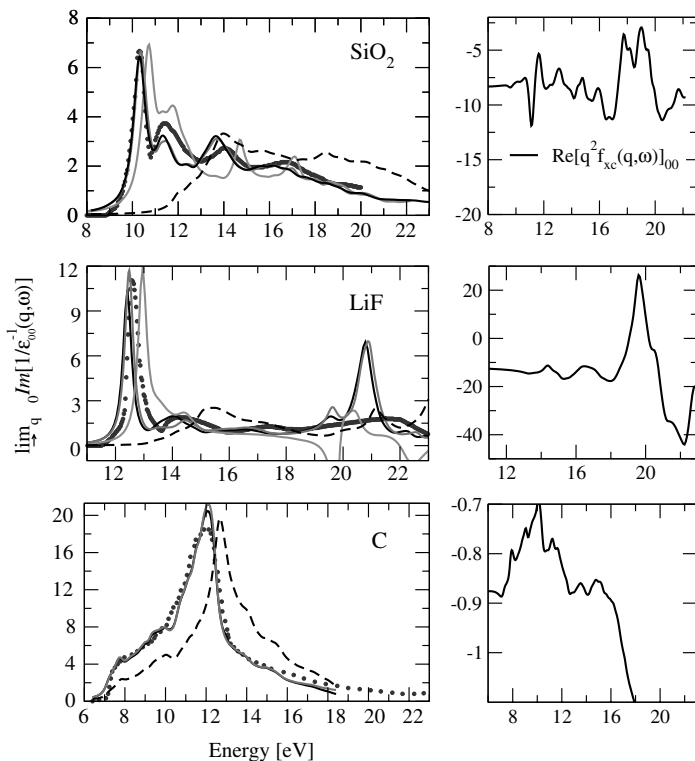


Fig. 20.4. *Left:* Calculated optical absorption spectra within the BSE (*continuous line*) and the new TDDFT xc kernel derived from the BSE (*dashed line*; nearly indistinguishable from the *continuous line*). The comparison between the two theoretical approaches and with experiment (*dots*) is excellent. We also provide the independent-quasiparticle response (GW-RPA; *dashed-dotted line*). *Right:* Frequency dependence of the head of f_{xc} (note the different scale for SiO₂, LiF and C) (Adapted from [Marini 2003b])

Now it is mandatory to address whether or not the description of strongly bound excitons within the TDDFT formalism is possible. This goal has been achieved using a frequency dependent and spatial nonlocal f_{xc} (see [Marini 2003b]) and the detailed derivation in Chap. 10 of this book). For all the materials discussed above where the LRC model work quite well, it is easy to show that the full kernel gives even better description of the BSE results than the simple model. Furthermore, it also works for wide band-gap insulators where the LRC model completely fails as showed for the optical absorption and electron-energy loss spectra of LiF, SiO₂ and diamond reproduces quite well the Bethe-Salpeter results and experiments (see Fig. 20.4). In these three systems the role of excitonic effects in the optical spectrum and EELS has been already analyzed within the BSE [Chang 2000, Benedict 1998a, Rohlfing

2000b, Arnaud 2001]. SiO_2 is characterized by four strong excitonic peaks at 10.3, 11.3, 13.5, and 17.5 eV, none of them below the QP gap of 10.1 eV, except for a bound triplet exciton optically inactive. Moreover, the exciton at 10.3 eV corresponds to a strongly correlated resonant state with a large degree of spatial localization (2–3 bond lengths) [Chang 2000]. The spectrum of LiF is dominated by a strongly bound exciton (~ 3 eV binding energy) [Benedict 1998a, Rohlfing 2000b, Arnaud 2001]. Last, in diamond, the electron–hole interaction produces a drastic modification of the independent QP spectrum by shifting optical oscillator strength from high to low energies. Furthermore, the head of f_{xc} is strongly frequency dependent in order to describe the high-energy features of the spectra (see inset in Fig. 20.4). This illustrates why the simple static-LRC model failed for the description of the wide-band gap insulators LiF and SiO_2 .

A similar situation occurs when studying surfaces, often characterized by strong excitons involving the localized surface states. Calculations carried out for $\text{Si}(111)2 \times 1$ [Rohlfing 1999b] have shown that the surface optical spectrum at low frequencies is dominated by a surface state exciton which has a binding energy that is an order of magnitude bigger than that of bulk Si, and one cannot interpret the experimental spectrum without considering excitonic effects. Very recently Pulci et al. [Pulci 2005] have demonstrated that a proper description of this bound exciton can be obtained using TDDFT with the above described f_{xc} . This completes the scenario, clearly confirming the robustness and wide-range of applicability of this new xc kernel in three and two-dimensional systems.

To conclude this section we show the calculated EELS of LiF (Fig. 20.5) for a *finite transfer momentum* \mathbf{q} along the ΓX direction, where previous BSE calculations and experimental results are available [Caliebe 2001]. This is a stringent test as the description of EELS needs causal response functions, including the anti-resonant part [Marini 2003b]. The results of this causal f_{xc} -calculation are presented in Fig. 20.5 for a 1st order (green line) and a 2nd order (red line) f_{xc} . While a first order, causal f_{xc} gives very good results, almost perfect agreement with BSE results is restored considering the second order correction to f_{xc} . This is not surprising as nothing ensures the same level of cancellation in the higher order expansion of resonant and causal functions. However, the final agreement with experimental data is anyway very good even at the first order. This is important for the predictive power of the many-body f_{xc} kernel for applications in low-dimensional structures.

In all these calculations it turns out that both spatial nonlocality and frequency dependence of the f_{xc} kernel are important in order to properly describe excitonic effects in the optical and electron energy-loss spectra. Still, quasiparticle effects need to be embodied properly within this approximated TDDFT scheme. More work needs to be done along this line.

As discussed in Chap. 10 of the present book, the perturbative kernel allows to handle the loss function as well as lifetime effects in wide-band

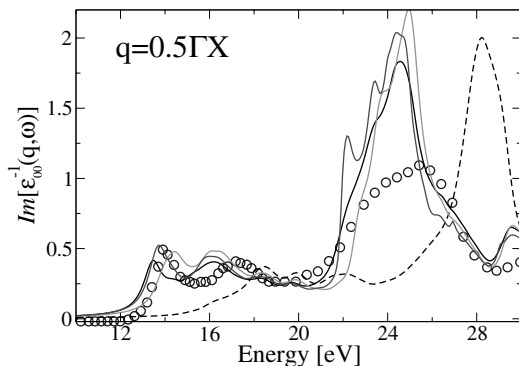


Fig. 20.5. Calculated EELS of LiF for a momentum transfer of $q = 0.5\Gamma X$: BSE (full line), 1st order f_{xc} (dot-dashed line), 2nd order f_{xc} (dashed line), and independent-QP (dots). Experiment (circles) are taken from [Caliebe 2001] (Adapted from [Marini 2003b])

gap insulators [Marini 2004]. In conclusion, we have provided compelling evidence of the good performance of the many-body derived f_{xc} kernel to describing the optical absorption and electron energy-loss spectra (for arbitrary q -momentum transfer) of bulk systems.

20.3 Applications to One Dimensional Systems and Molecules

In any finite system subject to an electric field, there is accumulation of charge at the surface, which induces a counter-field inside the sample. It is not possible for any local (or semi-local) functional of the density to describe the counter-field produced by the macroscopic polarization of the system [Gonze 1995b, Gonze 1997b, Gonze 1997a, Resta 1994, Ortiz 1998]. To circumvent this problem, it was proposed to use as an extra dynamical variable the surface charge, or equivalently the macroscopic field produced by that charge [Bertsch 2000b]. Another way to take into account the macroscopic polarization is by the current response of the system within a time-dependent current-density functional formalism [de Boeij 2001, van Faassen 2003a]. Those approaches have been discussed at length in other chapters of the present Part IV, therefore we will present here results obtained for one-dimensional systems and small molecules [Varsano 2005] by using the previous many-body xc kernel that has been shown to work for solids. The rationale for this choice is that the Bethe-Salpeter approach has been valuable in explaining and predicting the quasiparticle excitations and optical response of reduced dimensional systems and nanostructures. This is because Coulomb interaction effects in general are more dominant in lower

dimensional systems owing to geometrical and symmetry restrictions. As illustrated below, self-energy and electron-hole interaction effects can be orders of magnitude larger in nanostructures than in bulk systems made up of the same elements.

A good example of reduced dimensional systems are the conjugated polymers. The optical properties of these technologically important systems are still far from well understood when compared to conventional semiconductors. In particular, all simple local and gradient corrected functionals fail completely in describing the linear and nonlinear polarizabilities of long molecular chains [van Gisbergen 1999b, de Boeij 2001, van Faassen 2003a]. This failure in describing the hyperpolarizabilities has been traced back to the field counteracting term that appears, for example, in exact-exchange calculations or in orbital-dependent functionals, but that is completely absent in LDA or GGA functionals. Current density functional approaches also seem to solve, in part, this problem [de Boeij 2001, van Faassen 2003a]. Indeed, the use of the nonlocal and frequency-dependent f_{xc} derived from the Bethe-Salpeter equation restores the good agreement between the calculated polarizabilities and experimental data. Furthermore, it is able to describe also the H_2 -linear chain where the current DFT approach fails.

To illustrate the discussion we show, in Fig. 20.6, the optical absorption spectra of a prototype polymer: polyacetylene. We see that each of the 1D van Hove singularities in the interband absorption spectrum is replaced by a series of sharp peaks due to excitonic states. The lowest optically active exciton is a bound exciton state (singlet-excitation of π - π^* character) but the others are strong resonant exciton states. The peak structure agrees very well with experiment. The resonant part of f_{xc} reproduces very well the BSE results [Rohlfing 1999a] (and experiments). Again this shows the robustness of the f_{xc} for describing low-dimensional structures.

Furthermore, in Fig. 20.7 we show the computed spectra for a finite-system: the molecular unit of polyacetylene. For this finite system we see again that the resonant part of the xc kernel describes very well the BSE calculation (also resonant). However, in contrast to the infinite one-dimensional polymer, for this finite unit the coupling terms of the BSE equation are important accounting for a ~ 1 eV shift to lower energies of the main singlet-exciton peak (the upper part of the spectra is less sensitive to the coupling terms). In this case, the full causal f_{xc} also gives rise to a red-shift of the spectra but not enough to cope with the full coupling term in the BSE. This is an indication that we need to go beyond a first order xc kernel, an indication that has been also observed in the description of the electron-energy loss function of LiF [Marini 2003b] where the causal response needs a higher order f_{xc} in order to match the equivalent BSE results. Still, we can conclude that the first-order many-body f_{xc} is able to account for excitonic effects in one-dimensional structures, but higher orders are needed in zero-dimensional structures (molecules).

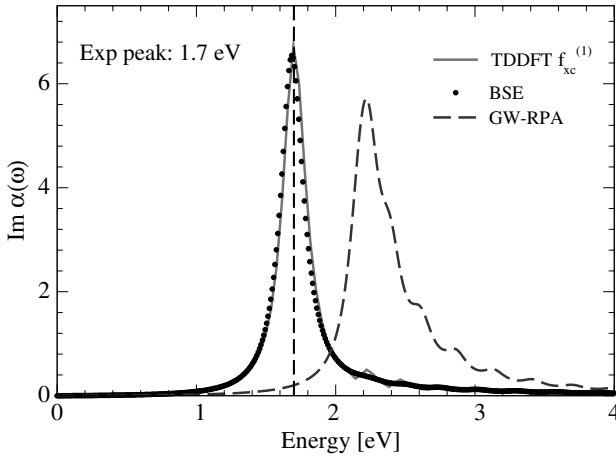


Fig. 20.6. Calculated optical absorption spectra of polyacetylene compared with experiments (*vertical dashed-line*). Clearly, the TDDFT calculation using the many-body f_{xc} is in good agreement with experiments as well as with the BSE calculation (*dots*). We also show the results of an RPA calculation using the GW quasiparticles energies (*dashed line*) to illustrate the impact of the electron-hole interaction in this one-dimensional system (Adapted from [Varsano 2005])

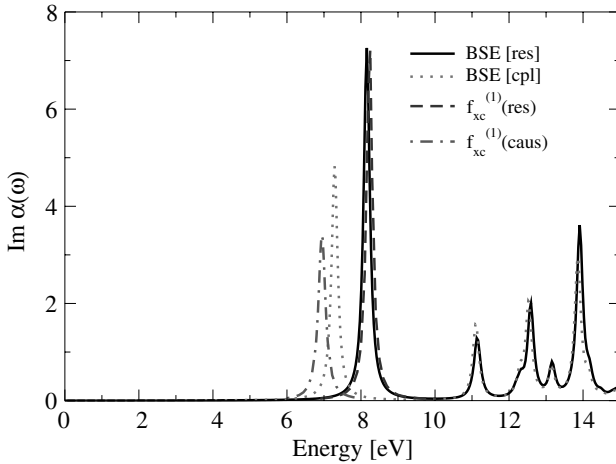


Fig. 20.7. Calculated optical absorption spectra of a single unit of the polyacetylene polymer. We compare the resonant and full BSE calculation with the TDDFT results using the resonant or the causal f_{xc} kernels (Adapted from [Varsano 2005])

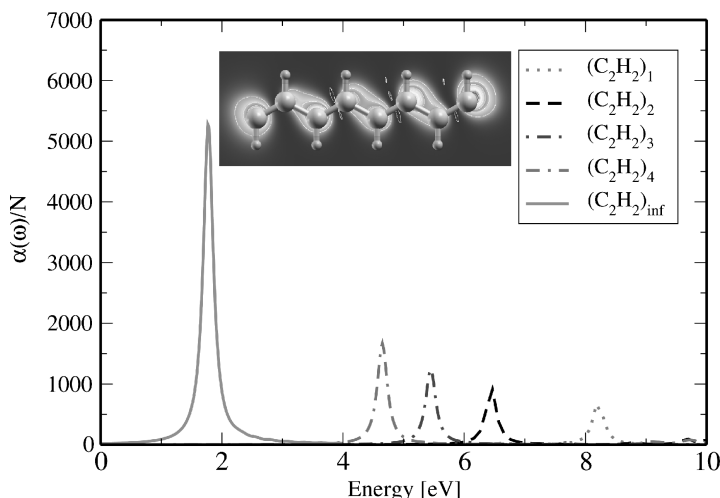


Fig. 20.8. Optical absorption spectra of the infinite chain of polyacetylene compared with the spectra for four different finite chains formed with different number of polyacetylene units. The figure illustrates the evolution of the main excitonic peak from about 7 eV in the monomer to 1.7 eV [Leising 1988] in the polymer chain. The inset shows the calculated excitonic wavefunction corresponding to the main absorption peak of the four-unit polyacetylene chain: we plot the probability of finding an electron when the hole is located at the left part of the chain (the probability maximum appears at the other side of the chain) (Adapted from [Varsano 2005])

Now we can make contact with the previous discussion of the static polarizability of long-molecular chains. First, we see that the optical spectra shifts from being dominated by a transition at about 7 eV (monomer) to one at 1.7 eV. This evolution with the number of monomers is monotonic and gives rise to the increase in polarizability (or equivalent to the decrease of the major absorption peak, as shown in Fig. 20.8). In particular, when the size of the polymer is larger than the localization length of the exciton (of the order of 100 Å), then the spectra becomes stable (no quantum confinement effects in the excitonic binding energy)⁵. At this point, the polarizability of the chain increases linearly with the number of monomer units. For smaller lengths, the polarizability increases faster but with smaller values than the corresponding LDA or GGA, in agreement with experiments and previous

⁵ This is clearly illustrated in the inset of Fig. 20.8 where the exciton wavefunction for the four unit polyacetylene chain is plotted. As the size of the molecule is smaller than the localisation length of the bulk exciton, then for if the hole is located on the right hand side the maximum probability for the electron is at the other extreme of the chain. This clearly creates a counteracting field that tends to reduce the polarisability.

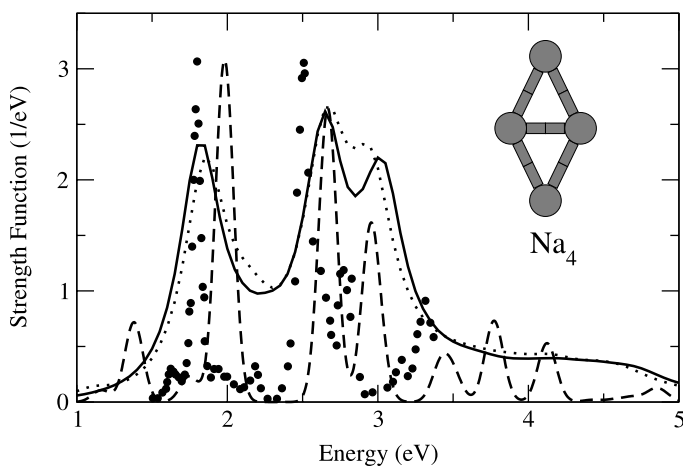


Fig. 20.9. Calculation of the optical absorption (that is proportional to the strength function) of a Na_4 cluster using the BSE scheme (*dashed line*) [Onida 1995] and with TDDFT using different kernels [Marques 2001]: TDLDA (*solid line*), exact-exchange (*dotted line*). *Filled dots* represent the experimental results from [Wang 1990a] (Adapted from [Onida 2002])

calculations [van Gisbergen 1999b, de Boeij 2001, van Faassen 2003a]. A similar trend has been obtained for the H_2 -chain [Varsano 2005]; the BSE results for the polarizability per H_2 unit are very close to Hartree-Fock and much lower than the LDA, GGA or current DFT (as it fails for this hydrogen chain [de Boeij 2001, van Faassen 2003a]). In summary, this BSE-derived scheme accounts for the presence of the counteracting field that is responsible for the lower static linear and nonlinear polarizabilities of the molecular chains [van Gisbergen 1999b]. Still work needs to be done to improve the description of higher-order correlation effects by f_{xc} .

Another example of low-dimensional systems are clusters. In Fig. 20.9, we show some results on the optical spectra of the Na_4 cluster calculated using the BSE approach as well as those from TDLDA and experiment. The measured spectrum consists of three peaks in the 1.5–3.5 eV range and a broader feature around 4.5 eV. The agreement between results from TDDFT and BSE calculations is very good. The comparison with the experimental peak positions is also quite good, although the calculated peaks appear slightly shifted to higher energies. The LDA kernel is a good approximation of the xc kernel of small sodium clusters. Good agreement has been obtained for other small semiconductor and metal clusters [Onida 2002] as well as biomolecules [Marques 2003a].

The above are just several selected examples, given to illustrate the current status in *ab initio* calculations of optical properties of materials. Similar results have been obtained for the spectroscopic properties of many other

moderately correlated electron systems, in particular for semiconducting systems, to a typical level of accuracy of about 0.1 eV.

Dimensionality Effects

Just to conclude this section we want to illustrate the effect of dimensionality and electron-hole attraction in a given material. In order to do that we show in Fig. 20.10 the recent results obtained by [Wirtz 2006] for Boron Nitride (BN) compounds where the transition from the bulk hexagonal layered structure to the sheet to the nanotubes, i.e, from three to two to one dimensions, it is highlighted. The optical properties of these tubes are found to be quite unusual and cannot be explained by conventional theories. Because of the reduced dimensionality of the nanotubes, many-electron (both quasiparticle and excitonic) effects have been shown to be extraordinarily important in both carbon [Spataru 2004] and BN nanotubes [Wirtz 2006, Park 2005].

In Fig. 20.10 we compare the results of a simple RPA calculation of the optical absorption spectra with the BSE results (that would be equivalent to the

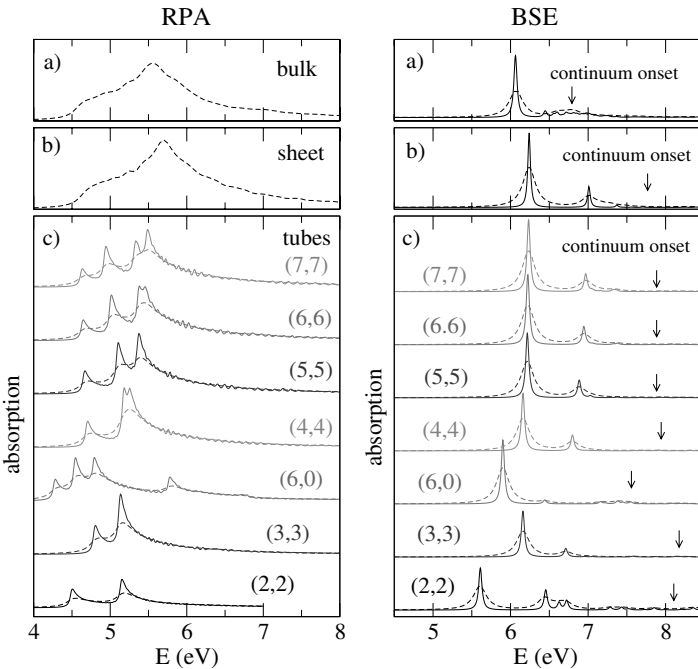


Fig. 20.10. Calculated optical absorption spectra of (a) hBN, (b) BN-sheet, and (c) six different BN tubes with increasing diameter d . The onset of continuum excitations is denoted by the vertical arrow. We compare the results of the BSE approach (*right hand side*) with the RPA (*left hand side*). Light polarization is parallel to the plane/tube axis, respectively (Adapted from [Wirtz 2006])

ones obtained using the many-body f_{xc}). Comparing the two figures a striking effect is observed: the electron-hole attraction modifies strongly the independent particle spectra (RPA) concentrating most of the oscillator strength into one active excitonic peak. The position of this peak seems rather insensitive to the dimensionality of the system in contrast to the RPA calculation where the shape of the spectra depends quite strongly on the tube diameter (the effect becomes smaller for very large tube diameters and it converges to the sheet and bulk values). The main effect of the dimensionality appears in the onset of the continuum excitations and the set of excitonic series above the main active peak. Thus, the binding energy for the first and dominant excitonic peak depends sensitively on the dimensionality of the system varying from 0.7 eV in the bulk BN to 3 eV in the hypothetical (2, 2) tube. However, the position of the first active excitonic peak is almost independent of the tube radius and system dimensionality. The reason for this subtle cancellation of dimensionality effects in the optical absorption stems from the strongly localized nature of the exciton (Frenkel-type) in BN systems [Wirtz 2006]. This band-gap constancy is in agreement with experiments [Arenal 2005] and has implications for the application of BN tubes for photoluminescence devices.

We remark that dimensionality effects would be more visible in other spectroscopic measurements as photoemission spectroscopy, where we mainly map the quasiparticle spectra, and this (as the exciton binding itself) is sensitive to the change in screening going from the tube to the sheet to bulk hBN [Wirtz 2006]. In particular the *quasi-particle band-gap* will vary strongly with dimensionality (opening as dimensionality reduces). The situation is different to the case of carbon nanotubes, where also excitonic effects are very important but also they depend on the specific nature of the tube [Spataru 2004].

20.4 Summary

We have discussed applications of an ab initio approach to calculating electron excitation energies, optical spectra, and exciton states in real materials following a many-body derived xc functional for TDDFT. The approach is based on evaluating the one-particle and the two-particle effects in the optical excitations of the interacting electron system, including relevant electron self-energy and electron-hole interaction effects at the GW approximation level (mimicked by an effective two-point xc kernel). It provides a unified approach to the investigation of both extended and confined systems from first principles. Various applications have shown that the method is capable of describing successfully the spectroscopic properties of a range of systems including semiconductors, insulators, surfaces, conjugated polymers, small clusters, and nanostructures. The agreement between theoretical spectra and data from experiments such as photoemission, tunneling, optical and related measurements is in general remarkably good for moderately correlated electron systems.

The main drawback in the many-body-based schemes is that we need to start from a *GW*-like quasiparticle calculation instead of the Kohn-Sham band-structure. As a matter of principle, both the quasiparticle shift as well as the redistribution of oscillator strength (including creation of new poles) due to excitonic effects (electron-hole attraction) should be accounted for by the nonlocal and frequency dependent f_{xc} kernel. However, until now we have been able to produce relatively good kernels that reproduce the effect of excitons in the response function but fail to include the quasiparticle shift. More developments are needed in the future to have a fully DFT-based theory that can be applied to both ground-state and excite-state properties. One appealing way are the orbital-dependent functionals derived from variational many-body formalism for the total energy (Φ and Ψ derivable functionals) [Almbladh 1999]. Preliminary results using the *GW* self-energy to build the total-energy functional and ulterior xc potential and kernel have been done for Si and LiF [Gruning 2005]. This approach includes the proper derivative discontinuity of the potential, being the corresponding Kohn-Sham gap very close to the standard local density approximation one. It also provides electron-hole effects and a reasonable description of the structural properties.

More work needs to be done along those lines and towards the inclusion of higher order vertex effects into the many-body description of electron-electron and electron-phonon interactions in order to have a more general ab initio theory of the spectra of weak and strongly correlated electronic systems.